

Evidence for the decay $B^0 \rightarrow K^+ K^- \pi^0$

V. Gaur,⁵⁵ G. B. Mohanty,⁵⁵ T. Aziz,⁵⁵ I. Adachi,¹² H. Aihara,⁶⁰ D. M. Asner,⁴⁶ V. Aulchenko,² T. Aushev,²¹ A. M. Bakich,⁵⁴ A. Bala,⁴⁷ K. Belous,¹⁸ V. Bhardwaj,³⁸ B. Bhuyan,¹⁴ G. Bonvicini,⁶⁶ A. Bozek,⁴² M. Bračko,^{31,22} T. E. Browder,¹¹ P. Chang,⁴¹ V. Chekelian,³² A. Chen,³⁹ P. Chen,⁴¹ B. G. Cheon,¹⁰ R. Chistov,²¹ K. Cho,²⁵ V. Chobanova,³² S.-K. Choi,⁹ Y. Choi,⁵³ D. Cinabro,⁶⁶ J. Dalseno,^{32,56} M. Danilov,^{21,34} Z. Doležal,³ Z. Drásal,³ A. Drutskoy,^{21,34} D. Dutta,¹⁴ K. Dutta,¹⁴ S. Eidelman,² H. Farhat,⁶⁶ M. Feindt,²⁴ T. Ferber,⁵ A. Frey,⁸ N. Gabyshev,² S. Ganguly,⁶⁶ R. Gillard,⁶⁶ Y. M. Goh,¹⁰ B. Golob,^{29,22} J. Haba,¹² H. Hayashii,³⁸ Y. Horii,³⁷ Y. Hoshi,⁵⁸ W.-S. Hou,⁴¹ H. J. Hyun,²⁷ T. Iijima,^{37,36} A. Ishikawa,⁵⁹ R. Itoh,¹² Y. Iwasaki,¹² T. Julius,³³ D. H. Kah,²⁷ J. H. Kang,⁶⁸ T. Kawasaki,⁴⁴ C. Kiesling,³² H. J. Kim,²⁷ J. B. Kim,²⁶ J. H. Kim,²⁵ K. T. Kim,²⁶ M. J. Kim,²⁷ Y. J. Kim,²⁵ K. Kinoshita,⁴ J. Klucar,²² B. R. Ko,²⁶ P. Kodyš,³ S. Korpar,^{31,22} P. Križan,^{29,22} R. Kumar,⁴⁹ T. Kumita,⁶² Y.-J. Kwon,⁶⁸ J. S. Lange,⁶ S.-H. Lee,²⁶ J. Li,⁵² Y. Li,⁶⁵ J. Libby,¹⁵ C. Liu,⁵¹ D. Liventsev,¹² P. Lukin,² D. Matvienko,² K. Miyabayashi,³⁸ H. Miyata,⁴⁴ N. Muramatsu,⁵⁰ R. Mussa,²⁰ E. Nakano,⁴⁵ M. Nakao,¹² M. Nayak,¹⁵ E. Nedelkovska,³² N. K. Nisar,⁵⁵ S. Nishida,¹² O. Nitoh,⁶³ S. Ogawa,⁵⁷ S. Okuno,²³ Y. Onuki,⁶⁰ W. Ostrowicz,⁴² P. Pakhlov,^{21,34} G. Pakhlova,²¹ H. Park,²⁷ H. K. Park,²⁷ T. K. Pedlar,³⁰ R. Pestotnik,²² M. Petrić,²² L. E. Piilonen,⁶⁵ M. Ritter,³² M. Röhrken,²⁴ A. Rostomyan,⁵ H. Sahoo,¹¹ T. Saito,⁵⁹ Y. Sakai,¹² S. Sandilya,⁵⁵ D. Santel,⁴ T. Sanuki,⁵⁹ Y. Sato,⁵⁹ V. Savinov,⁴⁸ O. Schneider,²⁸ G. Schnell,^{1,13} C. Schwanda,¹⁷ D. Semmler,⁶ K. Senyo,⁶⁷ O. Seon,³⁶ M. E. Sevir,³³ M. Shapkin,¹⁸ C. P. Shen,³⁶ T.-A. Shibata,⁶¹ J.-G. Shiu,⁴¹ A. Sibidanov,⁵⁴ F. Simon,^{32,56} J. B. Singh,⁴⁷ R. Sinha,¹⁹ P. Smerkol,²² Y.-S. Sohn,⁶⁸ A. Sokolov,¹⁸ E. Solovieva,²¹ M. Starič,²² M. Steder,⁵ M. Sumihama,⁷ T. Sumiyoshi,⁶² U. Tamponi,^{20,64} G. Tatishvili,⁴⁶ Y. Teramoto,⁴⁵ T. Tsuboyama,¹² M. Uchida,⁶¹ S. Uehara,¹² T. Uglov,^{21,35} Y. Unno,¹⁰ S. Uno,¹² S. E. Vahsen,¹¹ C. Van Hulse,¹ P. Vanhoefer,³² G. Varner,¹¹ K. E. Varvell,⁵⁴ V. Vorobyev,² M. N. Wagner,⁶ C. H. Wang,⁴⁰ P. Wang,¹⁶ X. L. Wang,⁶⁵ M. Watanabe,⁴⁴ Y. Watanabe,²³ K. M. Williams,⁶⁵ E. Won,²⁶ B. D. Yabsley,⁵⁴ Y. Yamashita,⁴³ S. Yashchenko,⁵ Y. Yusa,⁴⁴ V. Zhilich,² and A. Zupanc²⁴

(The Belle Collaboration)

¹University of the Basque Country UPV/EHU, 48080 Bilbao

²Budker Institute of Nuclear Physics SB RAS and Novosibirsk State University, Novosibirsk 630090

³Faculty of Mathematics and Physics, Charles University, 121 16 Prague

⁴University of Cincinnati, Cincinnati, Ohio 45221

⁵Deutsches Elektronen-Synchrotron, 22607 Hamburg

⁶Justus-Liebig-Universität Gießen, 35392 Gießen

⁷Gifu University, Gifu 501-1193

⁸II. Physikalisches Institut, Georg-August-Universität Göttingen, 37073 Göttingen

⁹Gyeongsang National University, Chinju 660-701

¹⁰Hanyang University, Seoul 133-791

¹¹University of Hawaii, Honolulu, Hawaii 96822

¹²High Energy Accelerator Research Organization (KEK), Tsukuba 305-0801

¹³Ikerbasque, 48011 Bilbao

¹⁴Indian Institute of Technology Guwahati, Assam 781039

¹⁵Indian Institute of Technology Madras, Chennai 600036

¹⁶Institute of High Energy Physics, Chinese Academy of Sciences, Beijing 100049

¹⁷Institute of High Energy Physics, Vienna 1050

¹⁸Institute for High Energy Physics, Protvino 142281

¹⁹Institute of Mathematical Sciences, Chennai 600113

²⁰INFN - Sezione di Torino, 10125 Torino

²¹Institute for Theoretical and Experimental Physics, Moscow 117218

²²J. Stefan Institute, 1000 Ljubljana

²³Kanagawa University, Yokohama 221-8686

²⁴Institut für Experimentelle Kernphysik, Karlsruher Institut für Technologie, 76131 Karlsruhe

²⁵Korea Institute of Science and Technology Information, Daejeon 305-806

²⁶Korea University, Seoul 136-713

²⁷Kyungpook National University, Daegu 702-701

²⁸École Polytechnique Fédérale de Lausanne (EPFL), Lausanne 1015

- ²⁹Faculty of Mathematics and Physics, University of Ljubljana, 1000 Ljubljana
³⁰Luther College, Decorah, Iowa 52101
³¹University of Maribor, 2000 Maribor
³²Max-Planck-Institut für Physik, 80805 München
³³School of Physics, University of Melbourne, Victoria 3010
³⁴Moscow Physical Engineering Institute, Moscow 115409
³⁵Moscow Institute of Physics and Technology, Moscow Region 141700
³⁶Graduate School of Science, Nagoya University, Nagoya 464-8602
³⁷Kobayashi-Maskawa Institute, Nagoya University, Nagoya 464-8602
³⁸Nara Women's University, Nara 630-8506
³⁹National Central University, Chung-li 32054
⁴⁰National United University, Miao Li 36003
⁴¹Department of Physics, National Taiwan University, Taipei 10617
⁴²H. Niewodniczanski Institute of Nuclear Physics, Krakow 31-342
⁴³Nippon Dental University, Niigata 951-8580
⁴⁴Niigata University, Niigata 950-2181
⁴⁵Osaka City University, Osaka 558-8585
⁴⁶Pacific Northwest National Laboratory, Richland, Washington 99352
⁴⁷Punjab University, Chandigarh 160014
⁴⁸University of Pittsburgh, Pittsburgh, Pennsylvania 15260
⁴⁹Punjab Agricultural University, Ludhiana 141004
⁵⁰Research Center for Electron Photon Science, Tohoku University, Sendai 980-8578
⁵¹University of Science and Technology of China, Hefei 230026
⁵²Seoul National University, Seoul 151-742
⁵³Sungkyunkwan University, Suwon 440-746
⁵⁴School of Physics, University of Sydney, NSW 2006
⁵⁵Tata Institute of Fundamental Research, Mumbai 400005
⁵⁶Excellence Cluster Universe, Technische Universität München, 85748 Garching
⁵⁷Toho University, Funabashi 274-8510
⁵⁸Tohoku Gakuin University, Tagajo 985-8537
⁵⁹Tohoku University, Sendai 980-8578
⁶⁰Department of Physics, University of Tokyo, Tokyo 113-0033
⁶¹Tokyo Institute of Technology, Tokyo 152-8550
⁶²Tokyo Metropolitan University, Tokyo 192-0397
⁶³Tokyo University of Agriculture and Technology, Tokyo 184-8588
⁶⁴University of Torino, 10124 Torino
⁶⁵CNP, Virginia Polytechnic Institute and State University, Blacksburg, Virginia 24061
⁶⁶Wayne State University, Detroit, Michigan 48202
⁶⁷Yamagata University, Yamagata 990-8560
⁶⁸Yonsei University, Seoul 120-749

We report a search for charmless hadronic decays of neutral B mesons to the final state $K^+K^-\pi^0$. The results are based on a 711 fb^{-1} data sample that contains $772 \times 10^6 B\bar{B}$ pairs, and was collected at the $\Upsilon(4S)$ resonance with the Belle detector at the KEKB asymmetric-energy e^+e^- collider. We find the first evidence for this decay with a significance of 3.5 standard deviations and measure its branching fraction as $\mathcal{B}(B^0 \rightarrow K^+K^-\pi^0) = [2.17 \pm 0.60(\text{stat}) \pm 0.24(\text{syst})] \times 10^{-6}$.

PACS numbers: 13.25.Hw, 14.40.Nd

The B -meson decay $B^0 \rightarrow K^+K^-\pi^0$ is suppressed in the standard model (SM) and thus offers a useful probe for new physics beyond the SM. Figure 1 shows typical Feynman diagrams that contribute to this decay. The dominant one is the color- and Cabibbo-suppressed $b \rightarrow u$ tree transition, followed by the internal W exchange diagram leading to $B^0 \rightarrow K^{*\pm}K^\mp$ with $K^{*\pm} \rightarrow K^\pm\pi^0$. The latter diagram dominates in the decay $B^0 \rightarrow K^+K^-$, for which only upper limits have been set [1–4]. This is in contrast to the related decays (having two kaons in the final state) that are already observed such as $B^0 \rightarrow K^0\bar{K}^0$, $B^+ \rightarrow K^0K^+$ [4, 5] and $B^+ \rightarrow K^+K^-\pi^+$ [6, 7], where

the $b \rightarrow d$ gluonic penguin amplitude can contribute as well [8].

The three-body decay $B^0 \rightarrow K^+K^-\pi^0$ has not yet been observed, with only one measured upper limit of $\mathcal{B}(B^0 \rightarrow K^+K^-\pi^0) < 9 \times 10^{-6}$ at 90% confidence level from the CLEO Collaboration [9]. Intermediate resonant modes that decay preferentially to this final state have also not been seen. A search for a related channel by Belle has set an upper limit of $\mathcal{B}(B^0 \rightarrow \phi\pi^0) < 1.5 \times 10^{-7}$ [10]. The latter mode is quite sensitive to possible beyond-the-SM contributions; a branching fraction of $\mathcal{O}(10^{-7})$ would constitute evidence for new physics [11]. No ex-

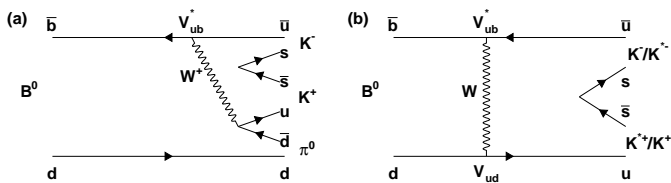


FIG. 1: Typical Feynman diagrams that contribute to the decay $B^0 \rightarrow K^+ K^- \pi^0$: (a) $b \rightarrow u$ tree and (b) internal W exchange.

perimental information is available for other potential resonance modes such as $K^*(892)^\pm K^\mp$, $K_0^*(1430)^\pm K^\mp$ and $f_0(980)\pi^0$. For the decay $B^0 \rightarrow K^*(892)^\pm K^\mp$, dominated by internal W exchange [Fig. 1(b)], the branching fraction is predicted to be in the range 10^{-8} to 10^{-7} [12–14].

Another motivation for the study of $B^0 \rightarrow K^+ K^- \pi^0$ comes from the observation of $B^+ \rightarrow K^+ K^- \pi^+$ by the BaBar Collaboration [6]. In particular, an unexpected structure is seen near $1.5 \text{ GeV}/c^2$ in the $K^+ K^-$ invariant-mass spectrum, which accounts for about half of the total events. Similar structures have also been observed in the Dalitz plots of $B^+ \rightarrow K^+ K^- K^+$ and $B^0 \rightarrow K^+ K^- K^0$ decays [15–17]. If these structures are due to a particular $K^+ K^-$ resonant state, it should show up in $B^0 \rightarrow K^+ K^- \pi^0$; on the other hand, if it is a reflection from the $b \rightarrow d$ penguin, it will not contribute to $K^+ K^- \pi^0$. Since the u and d quarks are spectators in the $b \rightarrow u$ tree diagram [Fig. 1(a)] for $B^+ \rightarrow K^+ K^- \pi^+$ and $B^0 \rightarrow K^+ K^- \pi^0$, respectively, one can estimate the branching fraction for the latter using the BaBar results. Assuming isospin symmetry and the $b \rightarrow u$ transition to be the main contributor to $B^0 \rightarrow K^+ K^- \pi^0$, we expect its branching fraction to be at the level of 3×10^{-6} , which is well within Belle’s reach.

Our results are based on a data sample, containing $772 \times 10^6 B\bar{B}$ pairs, collected at the $\Upsilon(4S)$ resonance with the Belle detector [18] at the KEKB asymmetric-energy e^+e^- (3.5 GeV on 8.0 GeV) collider [19]. The principal detector components used in the study are: a silicon vertex detector, a 50-layer central drift chamber (CDC), an array of aerogel threshold Cherenkov counters (ACC), a barrel-like arrangement of time-of-flight scintillation counters (TOF), and a CsI(Tl) crystal electromagnetic calorimeter (ECL). All these components are located inside a 1.5 T solenoidal magnetic field.

To reconstruct $B^0 \rightarrow K^+ K^- \pi^0$ decay candidates, we combine two oppositely charged kaons with a π^0 meson. Each track candidate must have a minimum transverse momentum of $100 \text{ MeV}/c$, and a distance of closest approach with respect to the interaction point of less than 0.2 cm in the transverse r - ϕ plane and less than 5.0 cm along the z axis, where the z axis is defined by the direction opposite the e^+ beam. Identification of charged

kaons is based on a likelihood ratio $R_{K/\pi} = \frac{\mathcal{L}_K}{\mathcal{L}_K + \mathcal{L}_\pi}$, where \mathcal{L}_K and \mathcal{L}_π denote the individual likelihoods for kaons and pions, respectively, calculated using specific ionization in the CDC, time-of-flight information from the TOF, and the number of photoelectrons from the ACC. A requirement $R_{K/\pi} > 0.6$ is applied to select both kaon candidates. The kaon identification efficiency is approximately 86% and the probability of misidentifying a pion as a kaon is 11%. We reconstruct π^0 candidates from photon pairs that have an invariant mass between 112 and $156 \text{ MeV}/c^2$, corresponding to $\pm 3.5\sigma$ around the nominal π^0 mass [20]. These photons are reconstructed from neutral clusters in the ECL with energy above 60 (100) MeV in the barrel (endcap) region. In addition, requirements on the π^0 decay helicity angle, $|\cos\theta_{\text{hel}}| < 0.95$, and the π^0 mass-constrained fit statistic, $\chi_{\text{mass}}^2 < 50$, are imposed. Here, θ_{hel} is the angle between one of the daughter photons and the B momentum in the π^0 rest frame.

B meson candidates are identified using two kinematic variables: beam-energy constrained mass, $M_{\text{bc}} = \sqrt{E_{\text{beam}}^2 - |\sum_i \vec{p}_i|^2}$, and energy difference, $\Delta E = \sum_i E_i - E_{\text{beam}}$, where E_{beam} is the beam energy, and \vec{p}_i and E_i are the momentum and energy, respectively, of the i -th daughter of the reconstructed B in the center-of-mass (CM) frame. We retain events with $5.271 \text{ GeV}/c^2 < M_{\text{bc}} < 5.289 \text{ GeV}/c^2$ and $-0.30 \text{ GeV} < \Delta E < 0.15 \text{ GeV}$ for further analysis. The M_{bc} requirement corresponds to approximately $\pm 3\sigma$ around the nominal B^0 mass [20]; we apply a looser window of $(-12\sigma, +6\sigma)$ around $\Delta E = 0$ because it is used in the fitter (as described below). The average number of B candidates found per event is 1.3. In events with multiple B candidates, we choose the one(s) whose π^0 has the lowest χ_{mass}^2 value. If more than one B candidate shares the same π^0 meson, the candidate yielding the best B^0 vertex fit is selected.

The dominant background is from the $e^+e^- \rightarrow q\bar{q}$ ($q = u, d, s, c$) continuum process. To suppress this background, observables based on the event topology are utilized. The event shape in the CM frame is more spherical for $B\bar{B}$ events and jet-like for continuum events. We employ a neural network [21] to combine the following six input variables: the Fisher discriminant formed from 16 modified Fox-Wolfram moments [22], the cosine of the angle between the B momentum and the z axis, the cosine of the angle between the B thrust and the z axis, the cosine of the angle between the thrust axis of the B candidate and that of the rest of the event, the ratio of the second to the zeroth order Fox-Wolfram moments (all of these quantities being calculated in the CM frame), and the separation along the z axis between the vertex of the B candidate and that of the remaining tracks. The training and optimization of the neural network are accomplished with signal and $q\bar{q}$ Monte Carlo (MC) simulated events. The signal MC sample is generated with the

EvtGen program [23] by assuming a three-body phase space. We require the neural network output (C_{NB}) to be above 0.2 to substantially reduce the continuum background. The relative signal efficiency due to this requirement is approximately 88%, whereas the continuum suppression achieved is close to 92%. The remainder of the C_{NB} distribution peaks strongly near 1.0 for signal, and thus we have difficulty in modeling it with an analytic function. However, its transformed variable

$$C'_{NB} = \log \left[\frac{C_{NB} - C_{NB,\min}}{C_{NB,\max} - C_{NB}} \right], \quad (1)$$

where $C_{NB,\min} = 0.2$ and $C_{NB,\max} = 1.0$, has a distribution with a Gaussian-like tail.

The background due to B decays via the dominant $b \rightarrow c$ transition is studied with an MC sample of a collection of such decays. The resulting M_{bc} distribution is found to peak strongly in the signal region. We also observe two peaks in the K^+K^- invariant-mass spectrum that corresponds to the contributions from (a) $D^0 \rightarrow K^+K^-$ peaking at the nominal D^0 mass [20], and (b) $D^0 \rightarrow K^-\pi^+$ with the peak shifted slightly from the D^0 mass owing to $K-\pi$ misidentification. To suppress these peaking contributions, we exclude candidates for which the invariant mass of the K^+K^- system lies in the range of [1846, 1884] MeV/ c^2 (about $\pm 5\sigma$ around the nominal D^0 mass). In the case of (b), we use the pion hypothesis for one of the tracks. The surviving events constitute the “generic $B\bar{B}$ ” background.

There are a few background modes that contribute in the M_{bc} signal region having the ΔE peak shifted to positive values. The so-called “rare peaking” background modes, arising mostly from $K-\pi$ misidentification, are identified with a $B\bar{B}$ MC sample in which one of the B mesons decays via $b \rightarrow u, d, s$ transitions with known or estimated branching fractions. The rare peaking background includes the $B^0 \rightarrow K^+\pi^-\pi^0$ nonresonant decay as well as possible intermediate resonant modes that result in the $K^+\pi^-\pi^0$ final state, such as $B^0 \rightarrow K^*(892)^0\pi^0$ and $B^0 \rightarrow K^*(892)^+\pi^-$. The events that remain after removing the signal and rare peaking components comprise the “rare combinatorial” background.

The signal yield is obtained with an unbinned extended maximum likelihood fit to the two-dimensional distributions of ΔE and C'_{NB} . We define a probability density function (PDF) for each event category j (signal, $q\bar{q}$, generic $B\bar{B}$, rare peaking, and rare combinatorial $B\bar{B}$ backgrounds):

$$\mathcal{P}_j^i \equiv \mathcal{P}_j(\Delta E^i) \mathcal{P}_j(C'_{NB}^i), \quad (2)$$

where i denotes the event index. Since the correlation between ΔE and C'_{NB} is found to be negligible, the product of two individual PDFs is a good approximation for the combined PDF. We apply a tight requirement on M_{bc}

rather than including it in the fitter because it exhibits an irreducible correlation with ΔE owing to shower leakage in the ECL. The extended likelihood function is

$$\mathcal{L} = \exp \left(- \sum_j n_j \right) \times \prod_i \left[\sum_j n_j \mathcal{P}_j^i \right], \quad (3)$$

where n_j is the yield of event category j . The correctly reconstructed (CR) and self-crossfeed (SCF) components of the signal are considered distinct in the fitter: their combined PDF is $n_{\text{sig}} \times [(1-f)\mathcal{P}_{\text{CR}} + f\mathcal{P}_{\text{SCF}}]$, where n_{sig} is the total signal yield and f is the SCF fraction, fixed to the MC expected value of 3%.

TABLE I: List of PDFs used to model the ΔE and C'_{NB} distributions for various event categories. G, AG, CB and Poly2 denote Gaussian, asymmetric Gaussian, Crystal-Ball [24] and second-order Chebyshev polynomial function, respectively.

Event category	ΔE	C'_{NB}
CR signal	CB+AG	3 AG
SCF signal	histogram	histogram
Continuum $q\bar{q}$	Poly2	AG
Generic $B\bar{B}$	Poly2	AG
Rare peaking $B\bar{B}$	2G	AG
Rare combinatorial $B\bar{B}$	histogram	3 AG

Table I lists the PDF shapes used to model the ΔE and C'_{NB} distributions for each event category. Distributions that are difficult to parametrize analytically are modeled with histograms. The yields for all event categories except the rare peaking $B\bar{B}$ background are allowed to vary in the fit. We fix the yield of the rare peaking $B\bar{B}$ component to the value calculated using the branching fraction measured in an amplitude analysis of $B^0 \rightarrow K^+\pi^-\pi^0$ [25]. The following PDF shape parameters of the $q\bar{q}$ background are floated: the two parameters of the second-order Chebyshev polynomial used for ΔE , and the mean and two widths of the asymmetric Gaussian function used to model C'_{NB} . The PDF shapes for signal and other background components are fixed to the corresponding MC expectations. We adjust the parameters of the signal ΔE and C'_{NB} PDFs to account for possible data-MC differences, according to the values obtained with a large-statistics control sample of $B^+ \rightarrow \bar{D}^0(K^+\pi^-\pi^0)\pi^+$. The same correction factors are also applied for the rare peaking $B\bar{B}$ background.

Figure 2 shows the ΔE and C'_{NB} projections of the fit applied to 39 066 candidate events. We obtain a signal yield of $n_{\text{sig}} = 299 \pm 83(\text{stat})$ events with a statistical significance of 3.8 standard deviations. The significance is calculated as $\sqrt{2 \log(\mathcal{L}_0/\mathcal{L}_{\text{max}})}$, where \mathcal{L}_0 and \mathcal{L}_{max} are the fit likelihood values with the signal yield set to zero and the best-fit case, respectively. The decay branching fraction is calculated as

$$\mathcal{B}(B^0 \rightarrow K^+K^-\pi^0) = \frac{n_{\text{sig}}}{N_{B\bar{B}} \times \varepsilon_{\text{rec}} \times r_{K/\pi}}, \quad (4)$$

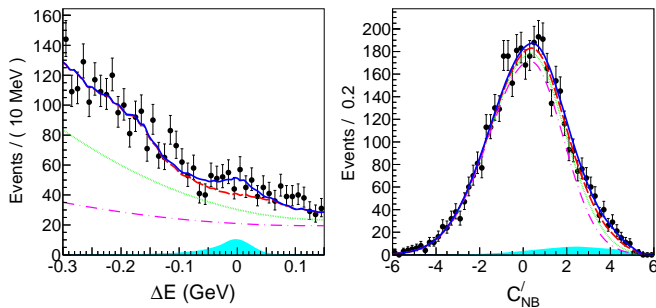


FIG. 2: (Color online). Projections of candidate events onto (left) ΔE for $C'_{NB} > 3$ and (right) C'_{NB} for $|\Delta E| < 30$ MeV. Points with error bars are the data, solid (blue) curves are the total PDF, dashed (red) curves are the total background, dotted (green) curves are the sum of continuum $q\bar{q}$ and generic $B\bar{B}$ backgrounds, dash-dotted (magenta) curves are the continuum $q\bar{q}$ background, and filled (cyan) regions show the signal.

where $N_{B\bar{B}}$ is the total number of $B\bar{B}$ pairs (772×10^6), ε_{rec} is the signal reconstruction efficiency (19.6%) obtained in the study described below, and $r_{K/\pi}$ denotes the kaon-identification efficiency correction factor that accounts for a small data-MC difference. It is given by

$$r_{K/\pi} \equiv \varepsilon_{K/\pi}^{\text{data}} / \varepsilon_{K/\pi}^{\text{MC}}, \quad (5)$$

where $\varepsilon_{K/\pi}^{\text{data}}$ ($\varepsilon_{K/\pi}^{\text{MC}}$) is the efficiency of the $R_{K/\pi}$ requirement in data (MC simulations). The $r_{K/\pi}$ value per kaon track is 0.95, resulting in a total $r_{K/\pi} = 0.95^2 = 0.90$ for two kaons. We have verified that the $R_{K/\pi}$ correction factor is almost constant over the Dalitz plot. For the branching fraction calculation presented in Eq. (4), we assume equal production of $B^0\bar{B}^0$ and B^+B^- pairs at the $\Upsilon(4S)$ resonance. The resulting value is

$$\mathcal{B}(B^0 \rightarrow K^+K^-\pi^0) = [2.17 \pm 0.60 \pm 0.24] \times 10^{-6}, \quad (6)$$

where the uncertainties are statistical and systematic, respectively. The contributions to the systematic uncertainty are discussed below and listed in Table II.

The uncertainties due to the PDF shape parameters are estimated by varying all fixed parameters by $\pm 1\sigma$. To assign a systematic error for the histogram PDF used to model ΔE for the rare combinatorial component, we carry out a series of fits by fluctuating each of the histogram bin contents according to the Poisson distribution. The spread of the fitted signal yields is taken as the systematic error. We also vary the yield of final states that dominantly contribute to that component according to their errors. As we use a fairly complex function (a sum of three asymmetric Gaussians) to model the signal C'_{NB} PDF shape, we evaluate possible systematics due to the uncertainty in the functional dependence by checking other alternatives. This systematic contribution

is denoted as ‘‘Signal C'_{NB} functional dependence’’ in Table II. The uncertainty due to the fixed (small) SCF fraction is estimated without knowing a priori how these SCF events vary across the Dalitz plot. We adopt a conservative approach to vary the SCF fraction by $\pm 50\%$ when calculating the associated systematic error. The potential fit bias is evaluated by performing an ensemble test comprising 200 pseudo-experiments, where the signal and rare peaking background components are embedded from the corresponding MC samples, and the PDF shapes are used to generate the data for the other event categories. We obtain an almost Gaussian pull distribution of unit width, and add the mean and error on the pull in quadrature for assigning the systematics. Uncertainty due to continuum suppression is derived with the control sample by comparing the nominal fit result with that obtained without any C_{NB} requirement. We estimate the error due to the M_{bc} requirement by varying its nominal selection threshold by the resolution. The $D^{*+} \rightarrow D^0(K^-\pi^+)\pi^+$ control sample is used to determine the systematic uncertainty due to the $R_{K/\pi}$ requirement. The systematic uncertainty due to π^0 reconstruction is evaluated by comparing data-MC differences of the yield ratio between $\eta \rightarrow \pi^0\pi^0\pi^0$ and $\eta \rightarrow \pi^+\pi^-\pi^0$. We use partially reconstructed $D^{*+} \rightarrow D^0(K_s^0\pi^+\pi^-)\pi^+$ decays to assign the systematic uncertainty due to charged-track reconstruction (0.35% per track). To account for the possible variation of efficiency across the Dalitz-plot distribution, we calculate a weighted signal reconstruction efficiency by fitting different regions of that distribution. The mean value is used to obtain the branching fraction and the error is taken as the systematic contribution due to the efficiency variation. The total systematic uncertainty is calculated by summing all these uncertainties in quadrature. To determine the significance of our measurement, we use a convolution of the statistical likelihood with a Gaussian function of width equal to the additive systematic errors that only affect the signal yield. The total significance, including these uncertainties, is 3.5 standard deviations.

To elucidate the nature of the observed signal, especially whether there are contributions from the decays with intermediate resonant states, we study the K^+K^- and $K^+\pi^0$ invariant mass distributions. We perform the $[\Delta E, C'_{NB}]$ two-dimensional fit in bins of the $m(K^+K^-)$ and $m(K^+\pi^0)$ distributions after applying the orthogonal requirements $m(K^+\pi^0) > 1.5 \text{ GeV}/c^2$ and $m(K^+K^-) > 2.0 \text{ GeV}/c^2$, respectively. These requirements suppress kinematic reflections. Figure 3 shows the resulting signal yields along with their statistical errors. With these data, we cannot make any definitive statement about possible intermediate K^+K^- resonances, including the structure seen by BaBar near $1.5 \text{ GeV}/c^2$ [6]. It is worth noting here that the recent LHCb study of $B^\pm \rightarrow K^+K^-\pi^\pm$ decays [7] has revealed an unidentified structure in the same mass range; however, it is only

TABLE II: Summary of various systematic uncertainties. The first and second horizontal blocks denote the additive and multiplicative systematic uncertainties, respectively.

Source	Uncertainties (%)	
Signal PDF	+3.4	-2.9
Generic $B\bar{B}$ PDF	+2.4	-3.1
Combinatorial background PDF	+1.3	-2.0
Peaking background PDFs	+1.7	-1.9
Fixed histogram PDF	+1.7	-2.0
Signal C'_{NB} functional dependence	+2.3	-2.3
Fixed SCF fraction	+1.7	-1.7
Fit bias	+2.4	-2.4
Continuum suppression	+2.2	-2.2
Requirement on M_{bc}	+1.5	-0.2
Kaon ID requirement	+1.9	-1.9
π^0 detection efficiency	+4.0	-4.0
Charged track reconstruction	+0.7	-0.7
Efficiency variation over Dalitz plot	+7.5	-7.5
Number of $B\bar{B}$ pairs	+1.4	-1.4
Total	+11.1	-11.3

present in B^+ events, giving rise to a large local CP asymmetry. Furthermore, we observe some excess of events around $1.4 \text{ GeV}/c^2$ in the $K^+\pi^0$ invariant-mass spectrum. A detailed interpretation will require an amplitude analysis with higher statistics that would be available at a next-generation flavor factory [26].

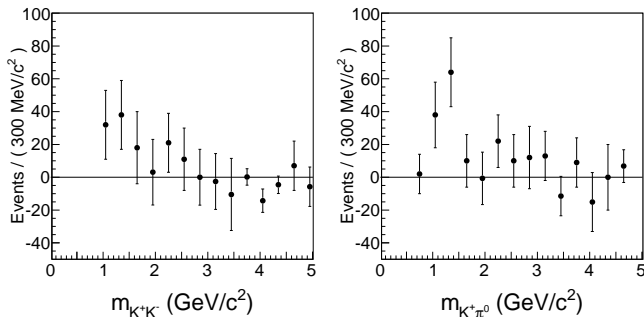


FIG. 3: Signal yield distributions as a function of (left) $m(K^+K^-)$ with $m(K^+\pi^0) > 1.5 \text{ GeV}/c^2$ and (right) $m(K^+\pi^0)$ with $m(K^+K^-) > 2.0 \text{ GeV}/c^2$. Each point is obtained from a two-dimensional $[\Delta E, C'_{NB}]$ fit.

In summary, we report measurement of the suppressed decay $B^0 \rightarrow K^+K^-\pi^0$ using the full $\Upsilon(4S)$ data sample collected with the Belle detector. We employ a two-dimensional fit for extracting the signal yield. Our measured branching fraction $\mathcal{B}(B^0 \rightarrow K^+K^-\pi^0) = [2.17 \pm 0.60(\text{stat}) \pm 0.24(\text{syst})] \times 10^{-6}$ constitutes the first evidence for the decay.

We thank the KEKB group for the excellent operation of the accelerator; the KEK cryogenics group for the efficient operation of the solenoid; and the KEK computer group, the National Institute of Informatics, and the

PNNL/EMSL computing group for valuable computing and SINET4 network support. We acknowledge support from the Ministry of Education, Culture, Sports, Science, and Technology (MEXT) of Japan, the Japan Society for the Promotion of Science (JSPS), and the Tau-Lepton Physics Research Center of Nagoya University; the Australian Research Council and the Australian Department of Industry, Innovation, Science and Research; Austrian Science Fund under Grant No. P 22742-N16; the National Natural Science Foundation of China under contract No. 10575109, 10775142, 10875115 and 10825524; the Ministry of Education, Youth and Sports of the Czech Republic under contract No. MSM0021620859; the Carl Zeiss Foundation, the Deutsche Forschungsgemeinschaft and the VolkswagenStiftung; the Department of Science and Technology of India; the Istituto Nazionale di Fisica Nucleare of Italy; The BK21 and WCU program of the Ministry Education Science and Technology, National Research Foundation of Korea Grant No. 2010-0021174, 2011-0029457, 2012-0008143, 2012R1A1A2008330, BRL program under NRF Grant No. KRF-2011-0020333, and GSDC of the Korea Institute of Science and Technology Information; the Polish Ministry of Science and Higher Education and the National Science Center; the Ministry of Education and Science of the Russian Federation and the Russian Federal Agency for Atomic Energy; the Slovenian Research Agency; the Basque Foundation for Science (IKERBASQUE) and the UPV/EHU under program UFI 11/55; the Swiss National Science Foundation; the National Science Council and the Ministry of Education of Taiwan; and the U.S. Department of Energy and the National Science Foundation. This work is supported by a Grant-in-Aid from MEXT for Science Research in a Priority Area (“New Development of Flavor Physics”), and from JSPS for Creative Scientific Research (“Evolution of Tau-lepton Physics”).

- [1] B. Aubert *et al.* (BaBar Collaboration), Phys. Rev. D **75**, 012008 (2007).
- [2] T. Aaltonen *et al.* (CDF Collaboration), Phys. Rev. Lett. **108**, 211803 (2012).
- [3] R. Aaij *et al.* (LHCb Collaboration), J. High Energy Phys. **10**, 037 (2012).
- [4] Y. T. Duh *et al.* (Belle Collaboration), Phys. Rev. D **87**, 031103 (2013).
- [5] B. Aubert *et al.* (BaBar Collaboration), Phys. Rev. Lett. **97**, 171805 (2006).
- [6] B. Aubert *et al.* (BaBar Collaboration), Phys. Rev. Lett. **99**, 221801 (2007).
- [7] R. Aaij *et al.* (LHCb Collaboration), Presented at the HCP conference in Kyoto, Japan, LHCb-CONF-2012-028 (2012).
- [8] Throughout this paper, inclusion of the charge-conjugate process is implied unless otherwise explicitly mentioned.
- [9] E. Eckhart *et al.* (CLEO Collaboration), Phys. Rev. Lett.

- 89**, 251801 (2002).
- [10] J. H. Kim *et al.* (Belle Collaboration), Phys. Rev. D **86**, 031101 (2012).
- [11] S. Bar-Shalom, G. Eilam, and Y. D. Yang, Phys. Rev. D **67**, 014007 (2003).
- [12] D. S. Du, H. J. Gong, J. F. Sun, D. S. Yang, and G. H. Zhu, Phys. Rev. D **65**, 094025 (2002); [Erratum-ibid. D **66**, 079904 (2002)].
- [13] M. Beneke and M. Neubert, Nucl. Phys. B **675**, 333 (2003).
- [14] L. Guo, Q. G. Xu, and Z. J. Xiao, Phys. Rev. D **75**, 014019 (2007).
- [15] A. Garmash *et al.* (Belle Collaboration), Phys. Rev. D **71**, 092003 (2005).
- [16] Y. Nakahama *et al.* (Belle Collaboration), Phys. Rev. D **82**, 073011 (2010).
- [17] J. P. Lees *et al.* (BaBar Collaboration), Phys. Rev. D **85**, 112010 (2012).
- [18] A. Abashian *et al.* (Belle Collaboration), Nucl. Instrum. Methods Phys. Res., Sect. A **479**, 117 (2002); also see the detector section in J. Brodzicka *et al.*, Prog. Theor. Exp. Phys. (2012) 04D001.
- [19] S. Kurokawa and E. Kikutani, Nucl. Instrum. Methods Phys. Res., Sect. A **499**, 1 (2003), and other papers included in this Volume; T. Abe *et al.*, Prog. Theor. Exp. Phys. (2013) 03A001 and following articles up to 03A011.
- [20] J. Beringer *et al.* (Particle Data Group), Phys. Rev. D **86**, 010001 (2012).
- [21] M. Feindt and U. Kerzel, Nucl. Instrum. Methods Phys. Res., Sect. A **559**, 190 (2006).
- [22] S. H. Lee *et al.* (Belle Collaboration), Phys. Rev. Lett. **91**, 261801 (2003).
- [23] D. J. Lange, Nucl. Instrum. Methods Phys. Res., Sect. A **462**, 152 (2001).
- [24] T. Skwarnicki, DESY Report No. F31-86-02 (1986), Appendix E.
- [25] J. P. Lees *et al.* (BaBar Collaboration), Phys. Rev. D **83**, 112010 (2011).
- [26] T. Abe *et al.* (Belle II Collaboration), arXiv:1011.0352 [physics.ins-det].